J Mater Sci (2008) 43:330–337
DOI 10.1007/s10853-007-1691-x

Microcracks with unexpected characteristics induced by CTE mismatch in two-phase model materials

Yoann Joliff · Joseph Absi · Marc Huger · Jean Claude Glandus

Received: 1 June 2006 / Accepted: 13 March 2007 / Published online: 17 October 2007

Abstract In order to study model microstructures representative of industrial refractory materials, this work is devoted to the elaboration and microstructural characterisation of two-phase model materials able to develop interfacial damage by thermal expansion mismatch between the matrix and inclusions. The studied materials are composed of a vitreous matrix surrounding dense alumina balls (Al_2O_3 99.9%). As expected, because of the not null dilatometric dissension ($\Delta\alpha < 0$ with $\alpha_{matrix} < \alpha_{inclusions}$), all the samples exhibit partial decohesions at the matrix-inclusions interfaces. But one also observes the presence of two types of unexpected cracks: straight cracks in the median plane between two inclusions and circular cracks around inclusions. Numerical, analytical and experimental tools were used to study the origin of such unexpected defects.

Introduction

The heterogeneity of industrial refractory materials results from their multiphased composition. The grains arrangement, the shape of aggregates and the microstructural defects such as porosity and cracks, make difficult the prediction of the mechanical and thermal behaviours of these materials. In order to understand the mechanical behaviour of real refractory materials, a first approach consists in simplify their microstructure to obtain model materials. Recently [1], we showed the interest of this model material in the case of two-phase model materials with fully cohesive interfaces (no thermal expansion mismatch between inclusions and matrix: $\Delta\alpha = 0$). In order to describe more precisely the microstructure of real refractory materials, this work is devoted to the case of heterogeneous model materials with partly cohesive: matrix/inclusions interfaces (non-null thermal expansion mismatch between inclusions and matrix: $\Delta\alpha \# 0$ with $\alpha_{matrix} < \alpha_{particles}$). As predicted by analytical models [2–5], the normal tensile stresses are maximum at the matrix-inclusions interfaces and can induce debonding phenomenon during the cooling stage of the sintering cycle. Indeed microscopic observations confirmed the presence of such decohesions, but also showed two other types of unexpected cracks in the matrix: straight cracks between two inclusions and circumferential cracks around inclusions. The first ones, which only appear when two inclusions are close, take place in the median plane between two inclusions. Their origin could be related to the uniaxial pressing, which induces heterogeneity in the compaction of the raw piece, and this heterogeneity plays an important role during the cooling stage of the sintering cycle. The seconds are always associated with a local debonding of the matrix-inclusions interfaces.

The present work studies the origins of these unexpected cracks using numerical, analytical and experimental tools.

Elaboration

The studied model materials are composed of a glass matrix containing spherical alumina inclusions. Although it is not a refractory material, a glass has been chosen as matrix, because its coefficient of thermal expansion can be

Y. Joliff (✉) · J. Absi · M. Huger · J. C. Glandus
GEMH, Ecole Nationale Supérieure de Céramique Industrielle, 47 à 73 avenue Albert Thomas, 87065 Limoges cedex, France
e-mail: y_joliff@ensci.fr

easily adjusted by means of its oxides content. Spherical inclusions are balls of dense alumina (99.9%) of 700 μm in diameter. The thermal and mechanical properties of the constituents are reported in Table 1. The glass frit, the alumina balls and the organic additives are mixed, and then pressed (45 MPa) at room temperature. Then, the green piece is sintered according to the thermal cycle described in Fig. 1a. After this stage of natural sintering, the remaining porosity is close to 5%. To decrease this value, samples are subjected to an uniaxial hot pressing (Fig. 1b). Finally, the samples exhibit a porosity lower than 1.5% whatever their inclusions content is (up to 40% in vol.).

Microscopy observations

After natural sintering, optical as well as electronic microscopy observations confirm the presence of the expected decohesions at the matrix/inclusion interfaces in the sintered materials (Fig. 2a). But they also show the presence of other damages in the bulk of the vitreous matrix (Fig. 2b, c). These unexpected microcracks are present in all the samples and their numbers vary according to the inclusions content. Two types of these unexpected defects are observed: the first one is a median microcracking between two balls (Fig. 2b) which appears only when inclusions are close one to each other and the second one is a circumferential matrix microcracking beyond the debonding interface (Fig. 2c). Similar damages were previously observed on other two-phase materials by different authors [6–7] (Fig. 3) who never propose any explanation about the origin of such defects.

Finally, it should be underlined that, in our case, no observation showed circumferential cracking without close interfacial decohesion.

The hot pressing significantly reduces the porosity (less than 1.5% after hot pressing), and attenuates the defects but not fully heal them.

Table 1 Thermal and mechanical properties of the constituents

	Designation	E (GPa)	ν	ρ (kg/m3)	α (K–1) [50–450 °C]
Alumina	Brace 700 μm	340	0.24	3300	7.6.E–6
Glass	Ferro 365/400	68	0.206	2400	4.6.E–6

Origin of unexpected microcracking

In our materials, the microscopic cracks are present before hot pressing. So, it may be thought that their origin lies in the two processing stages of uniaxial pressing and natural sintering. In order to validate this assumption, numerical models have been developed to understand the effects of:

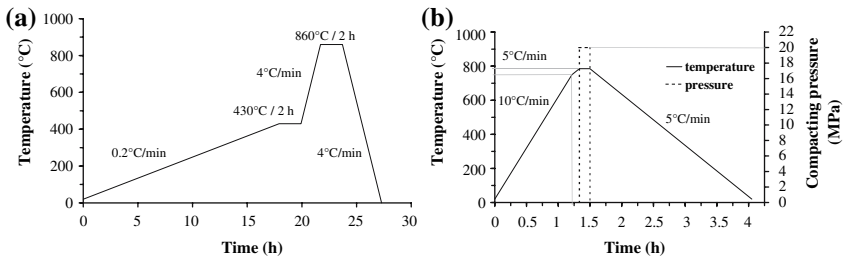

Fig. 1 Sintering (**a**) and thermo-compression (**b**) cycles

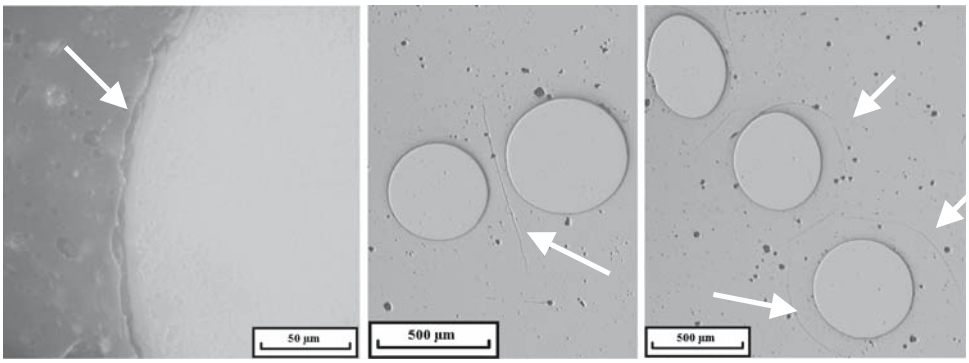

(a) Interfacial debonding zone **(b)** Microcrack between two close inclusions **(c)** Microcracks away from the interface

Fig. 2 Real model material (with 20% vol. of alumina balls) after natural sintering

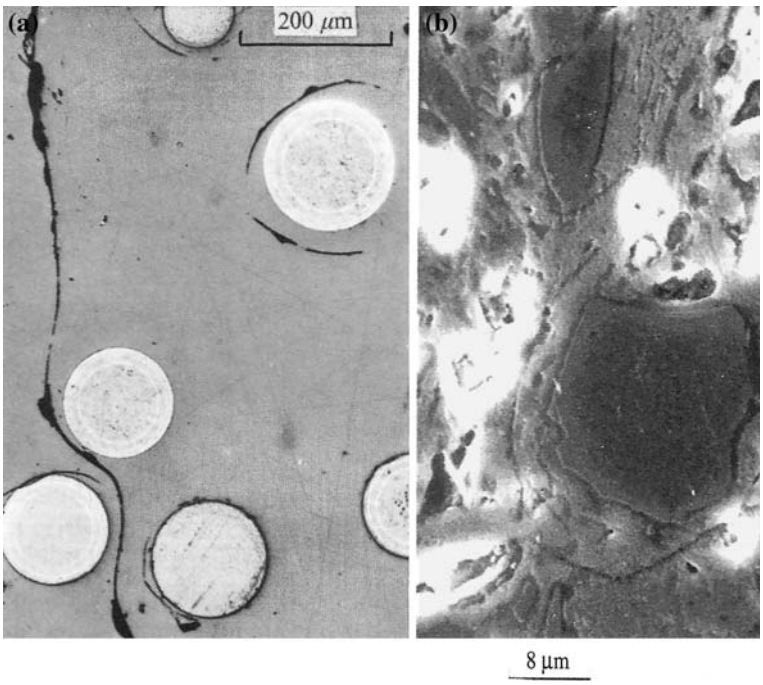

Fig. 3 Circumferential cracks around rigid particles in a ThO_2-sphere-in-glass composite [6] (**a**) and in a quartz grain in porcelain [7] (**b**)

– the compaction stage of glass frit by uniaxial pressing;
– the cooling stage of natural sintering.

Then experimental and analytical arguments, so as these numerical results have been used to justify the presence of the two types of unexpected defects previously shown.

Influence of the process

Compaction stage of glass frit by uniaxial pressing

The uniaxial pressing of a powder always generates a heterogeneous compaction of this one [8]. In our case, it may be thought that the addition of rigid particles can disturb much more the pressure field inside the glass powder during the pressing stage. Thus, a 2D numerical study of the stress field around particles was carried out using the finite elements method (Abaqus code) to validate this hypothesis. In the case of an uniaxial pressing (P_{comp} = 45 MPa) of a compliant matrix ($E_{softened\ matrix}$ = 10 GPa) containing in its centre a rigid inclusion ($E_{rigid\ particle}$ = 340 GPa), the calculated stress levels show a non-uniform pressure distribution in the mould. As expected, the use of a floating mould improves pressing by symmetrizing the pressure distribution but cannot homogenise this distribution around the inclusions (Fig. 4a). Many works showed the impact of the pressing process on the microstructure after sintering. Chartier et al. [9] studied the microstructure evolution during the heat treatment of a partly stabilised zirconia powder forming by dry pressing and tape casting. They observed a better homogeneity of the samples obtained by tape casting which exhibit a better densification. More recently, Mei et al. [10], in a similar study

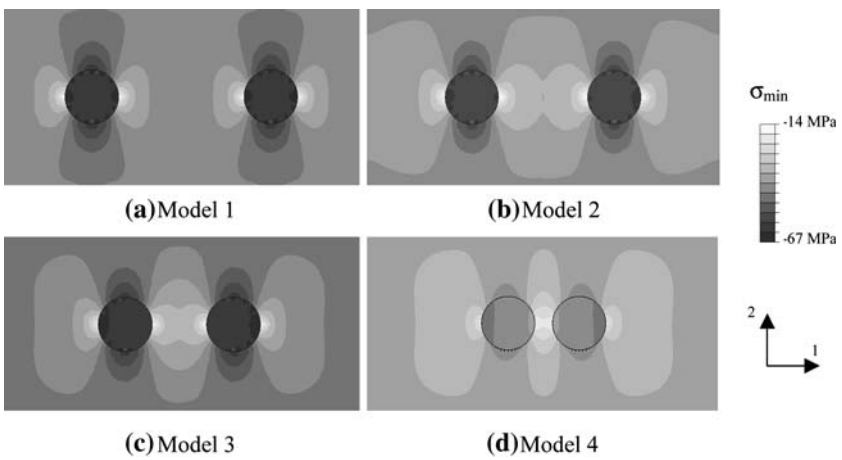

Fig. 4 Compaction stresses in a compliant matrix containing two rigid inclusions and subjected to a uniaxial pressing for 4 inter-inclusions distances

between the forming of a cordierite-based glass ceramic by slip casting and by dry pressing obtained similar conclusions. Thus, it appears that whatever the pressing technique is, the densification of a green material containing rigid particles will be unavoidably heterogeneous because dry pressing generates a strong pressure scattering in the vicinity of inclusions.

In order to understand the interactions between close particles during uniaxial pressing, several numerical models similar to the previous one but with two rigid inclusions were developed. The results show an heterogeneous distribution of the maximum principal stresses which vary according to the inter-inclusions distance (Fig. 4). In the matrix, a strong stress gradient exists in the vicinity of the rigid particles, which probably leads to a powder compaction gradient. The isovalues stress maps show a zone close to the matrix/inclusion interface where the stress level is about three times lower than the applied pressure (P_{comp} = 45 MPa). The size of this zone, small for distant particles (Fig. 4a), increases when the particles distance decreases (Fig. 4d). Moreover, the mean pressure between the two particles strongly decreases (from about –43 MPa for the Model 1 to –21 MPa for the Model 4, Fig. 5). At the same time, the stress gradient between the two particles also decreases when the inter-particles distance decreases

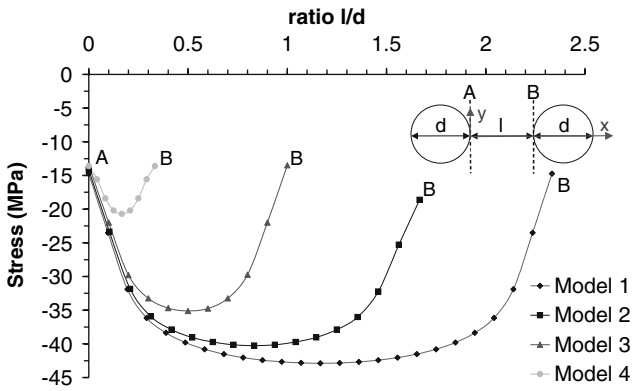

Fig. 5 Compaction stresses ($\sigma_{max.}$) in the matrix between two inclusions vs l/d ratio

($\Delta\sigma$ = 29 MPa for the Model 1; $\Delta\sigma$ = 7 MPa for the Model 4, Fig. 5). All these results show that, in presence of rigid inclusions, uniaxial pressing creates large scattering in the powders compaction able to induce a heterogeneous densification of the matrix during sintering.

Numerical models containing several inclusions randomly distributed allow to generalise these observations. Indeed, as shown by the Fig. 6, the phenomena previously observed (localised pressure deficit) in the case of two inclusions are not significantly disturbed by the presence of new inclusions in their vicinity.

Cooling stage of natural sintering

Many works deal with the heating of non-homogeneously compacted samples with or without rigid inclusions. In 1982, Evans [11] proposed a method to estimate the stresses arising during the sintering of green materials non-homogeneously densified. Later, Scherer [12] and Rahaman and Jonghe [13] studied the reliability of predicting tools of the stresses induced by the sintering of a two-phase material with rigid particles. These results show that the stress levels can be reliably predicted for inclusions contents lower than 10% (in volume). Beyond this critical value, the interactions between rigid particles cannot be neglected and a significant difference is observed between the computed and the experimental values. In 1995, Hong and Dharani [14] studied by the finite elements method the sintering of a not compacted powder with rigid particles so as its impact on the material densification. They show that the presence of rigid particles close one to the other delays the material densification. More recently, Boccaccini and Olevsky [15] showed that the sintering of a green sample containing rigid particles leads to a material exhibiting a gradient of density.

The present study has been chiefly focused on the cooling stage of the sintering cycle. Indeed, it is during this stage that cracking will be initiated because of the non-homogeneous densification induced by the pressing stage in the green samples. The literature [2–5] proposes many analytical models to predict the stress levels induced

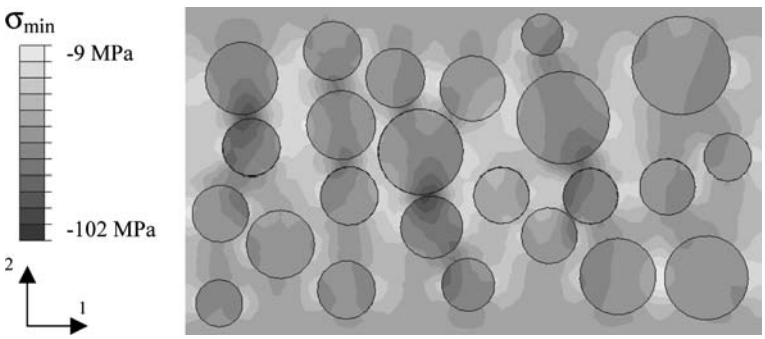

Fig. 6 Compaction stresses in a compliant matrix containing many rigid particles and subjected to a uniaxial pressing

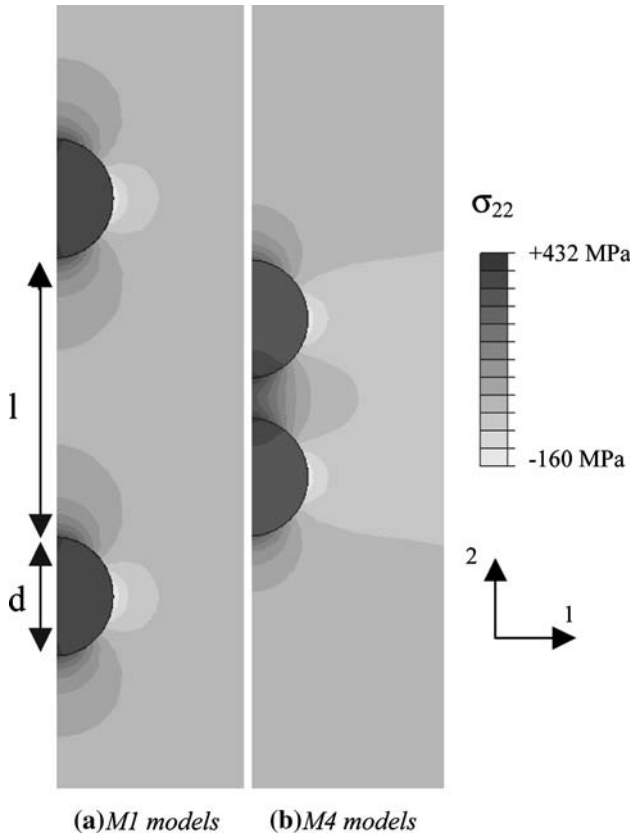

Fig. 7 σ_{22} stresses for two numerical models (thermal loading)

by cooling for a single particle within a matrix exhibiting a thermal expansion coefficient different from that of the inclusions. All these models show that the maximum stress level is always located at the matrix/inclusion interface.

In order to understand these damaging phenomena, we performed a qualitative numerical study of the isothermal cooling (from about 600 °C to 20 °C) of a glass matrix containing two alumina spherical inclusions (see physical properties in Table 1) more or less distant one from the other (Fig. 7). Then, using an analytical model [5], we predicted the stress at a given distance from the centre of the particle, for a given variation of temperature. The radial stress in the matrix is expressed by the formula (1).

$$\sigma_{rr}^{m} = \frac{1}{(r/r_0)^3} \frac{12\, G_m\, K_p\, (\alpha_m - \alpha_p)\, \Delta T}{4\, G_m + 3\, K_p} \quad (1)$$

where r is the distance between the particle's centre and the point where the stress is calculated in the matrix; r_0 is the radius of the particle; G_m, K_p, α_m and α_p are respectively, the shear modulus, the bulk modulus and the coefficients of the thermal expansion of the matrix (m) and the particle (p).

The results show (Fig. 8) that, between two inclusions, the maximum stress is located at the particles interfaces whatever the inter-inclusions distance is. Moreover, the numerical and analytical (1) results agree if the inter-particles distant are sufficiently large (Fig. 8), if this distance becomes lower than the particle diameter (Fig. 8), the assumption of a single particle postulated by the analytical models becomes invalid. In this case, the numerical computation, able to take into account the interactions between close inclusions, leads to more realistic stresses than the analytical models.

Median microcracking between two inclusions

The median microscopic crack observed on the Fig. 2b can be explained by the two previous results. When two inclusions are sufficiently distant one from the other (Model 1, Fig. 4), the compaction stress in the median zone between the two objects is approximately equal to the external pressure (in the present case, $\sigma_{comp} = 43$ MPa when $p_{ext} = 45$ MPa). Then, it can be thought that the compacting of this zone is quite full and that notable porosity cannot arise during sintering. Consequently, no cracking can develop if the stress level does not exceed the strength of dense matrix. On the other hand, if the distance between inclusions decreases to reach that described by the Model 4 (Fig. 4), the compaction stress in the median zone between inclusions becomes lower than half of the external pressure (here, $\sigma_{comp} = 21$ MPa when $p_{ext} = 45$ MPa). So, one can suppose that sintering will induce in this zone a significant porosity which gives rise to a local lowering of

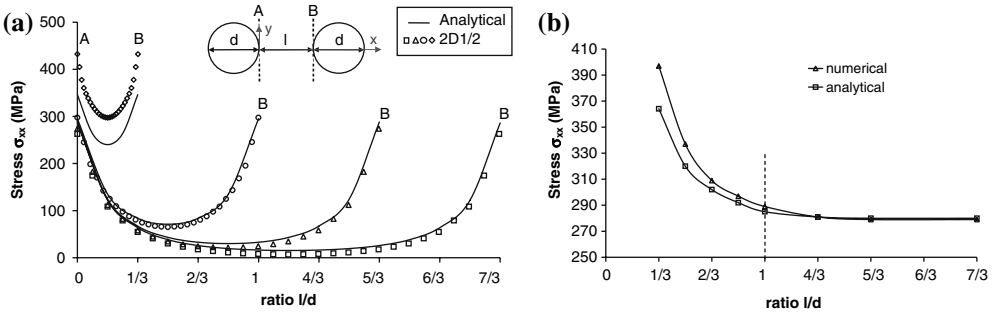

Fig. 8 (**a**) Thermal stresses σ_{xx} in the matrix between two inclusions vs l/d ratio. (**b**) Analytical and numerical interfacial thermal stresses vs l/d ratio

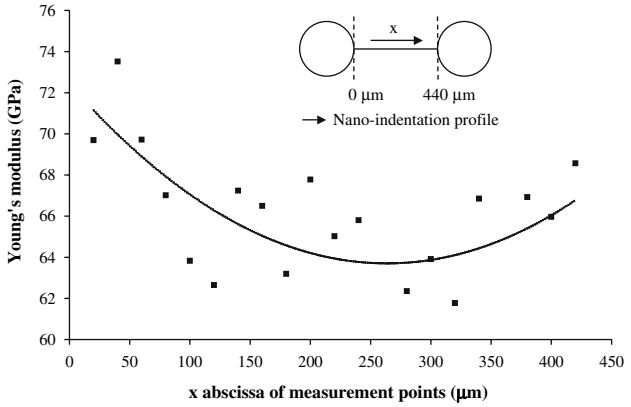

Fig. 9 Young's modulus vs distance between two close particles (nano-indentation measurements)

mechanical properties, especially of strength. Thus, cracking can occur for stress level lower to the strength of the dense matrix.

Moreover, during the sintering cooling stage, the stress distribution between two inclusions is strongly dependant on their distance, like illustrated by Fig. 8, which represents the stresses induced by an isothermal cooling. The stress which develops in the median zone is thus lower than the interfacial stress, but the material strength is also lowered in this zone. Thus cracking can occur in this zone if the strength decrease is larger than the stress decrease.

The problem is then to know the residual porosity in this zone in order to estimate the local strength of material. An analytical calculation being impossible, we implemented an indirect experimental method based on the calculation of the material Young's modulus by means of a set of nano-indentation measurements along a straight line between two inclusions.

The E values so measured are roughly fitted by a U shaped curve (Fig. 9), which qualitatively validates the postulated assumption. Unfortunately, these results exhibit a too significant noise to allow the calculation of local porosity. An improvement of the experimental technique is thus needed to obtain sufficiently fine values permitting the quantitative validation of the supposed origin of median cracking.

Circumferential microcracking around inclusions

In order to explain the origin of the circumferential cracks close to inclusions (Fig. 2c), a simple numerical model (a single spherical alumina inclusion centred in a cube of glass) was developed to describe the stress field induced by the sintering cooling. The sample is subjected to an isothermal cooling from the vitreous transition temperature (T_g = 600 °C) to the room temperature (T_{amb} = 20 °C). At the beginning of simulation ($T = T_g$), the matrix/inclusion contact is fully cohesive (obtained thanks to a permanent Tied contact type).

At the end of the first computing time step, the maximum stress is located at the matrix/inclusion interface (Fig. 10a). For a sufficient temperature drop (ΔT = 300 °C), the stress level at the interface reached the glass strength (σ_R = 45 MPa): thus, the first rupture (for a material free of defect) corresponds to a matrix/inclusion decohesion, induced by the radial tensile stresses at the interface (Fig. 10b).

A crack representating this partial decohesion is then introduced into the numerical model by the modification of the matrix/inclusion contact type and the thermal loading previously described is applied to this new model.

Because of the matrix/inclusion decohesion, a stress concentration arises at the crack tips and the principal stresses directions at these points rotate of about 55° regarding the inclusion radius (Fig. 11). So, the maximum tensile stress does not remain perpendicular to the interface and can lead to the matrix cracking (Fig. 12a, b).

These results show that the initial decohesion is able to induce a crack, which can then propagate along an arc in the matrix around the inclusion. The microscopic observations showing always both interfacial debonding and matrix cracking, numerical simulations take this fact into account and study the mutual influence of these two defects. This peripheral crack beside the interfacial decohesion tends to increase the instability of this latter, so as

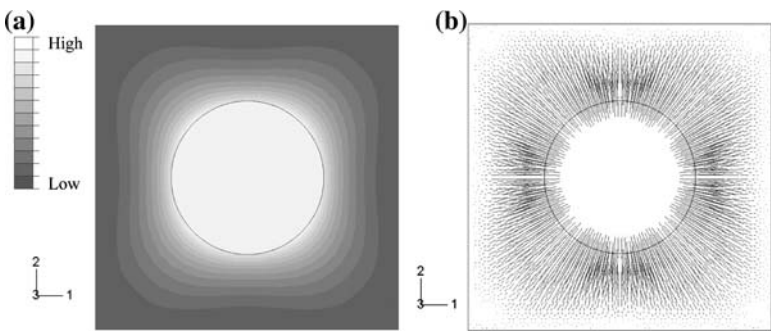

Fig. 10 Isovalues (**a**) and directions (**b**) of maximum principal stresses (isothermal cooling from 600 °C to 20 °C)

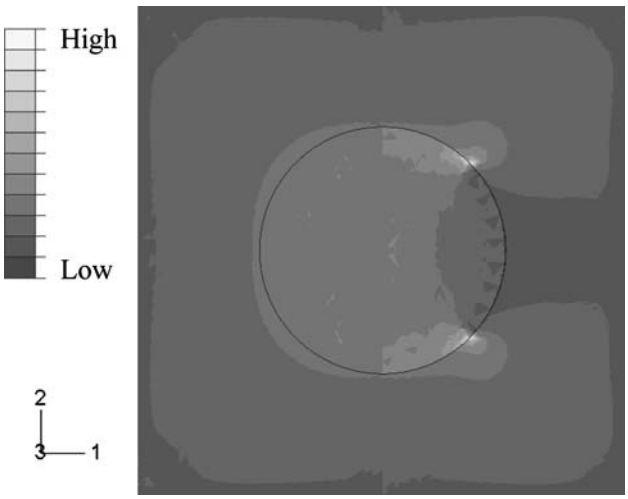

Fig. 11 Map of maximum principal stresses for a model material presenting a partial decohesion (isothermal cooling from 600 °C to 20 °C)

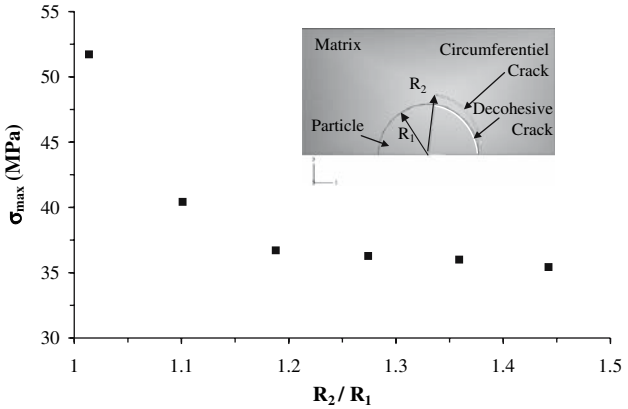

Fig. 13 Maximum principal stress between two cracks tips for ΔT = 100 °C

its propagation rate. But when this matrix crack is sufficiently far from the interface, its influence on the debonding propagation is negligible. The Fig. 13 illustrates the maximum stress calculated vs the distance between the two cracks tips for a given ΔT value (ΔT = 100 °C). Indeed, the numerical results show that when this distance becomes larger than the quarter of the inclusion radius, the two cracks can be considered as independent. Far from the matrix-inclusion interface, the tip of the circumferential crack is subjected to stresses lower than the glass strength and the crack propagation stops.

Conclusion

The processing of two-phase materials exhibiting a dilatation mismatch between the phases is rather difficult and the manufactured products must be carefully observed. At room temperature, the samples exhibit both partial decohesions at the matrix/inclusions interfaces and various types of unexpected cracks in the matrix. These defects are induced by the various processing stages such as pressing and sintering and an original mechanical explanation has been proposed for the origin of one of these defects. Many works describe the difficulty to compact and to sinter powder mixtures including rigid particles. During sintering, the non-uniformity of the pressure field leads to a heterogeneous densification of materials, which induces damage in the samples. Nano-indentation measurements between two particles show a significant Young's modulus decrease and so, qualitatively validate this assumption. The numerical simulations show that the initial decohesion induces a crack which can propagate along an arc in the matrix around the inclusion. These results show also the close dependence between the interfacial debonding and the circonferential cracking growth. A post hot pressing stage attenuates these defects but cannot fully heal them.

Consequently, when using analytical and numerical predicting tools, it will be necessary to use macroscopic homogenised mechanical and thermal properties, taking into account the pre-cracking of material.

Acknowledgements Yoann Joliff would like to express his gratitude towards the Limousin Region and the European Social Fund for financial support of the present work.

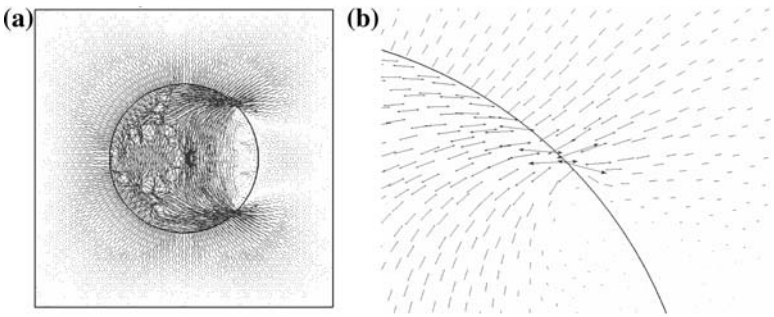

Fig. 12 Maximum principal stress directions in the model (**a**) and near the crack tip (**b**) for a model material presenting a partial decohesion (isothermal cooling from 600 °C to 20 °C)

References

1. Tessier-Doyen N (2003) Etude expérimentale et numérique du comportement thermomécanique de matériaux réfractaires modèles. Ph.D. thesis, University of Limoges, France
2. Hsueh CH, Becher PF, Sun EY (2001) J Mater Sci 36:255
3. Dean-Mo L, Jenny Winn E (2001) J Mater Sci 36:3487
4. Hsueh CH, Becher PF (1996) Mater Sci Eng A212:29
5. Lauke B, Schüller T, Beckert W (2000) Comput Mater Sci 18:362
6. Davidge RW, Green TJ (1968) J Mater Sci 3:629
7. Haussonne J M, Carry C, Bowen P, Barton J (2005) In: Traité des matériaux: céramiques et verres – Principes et techniques d'élaboration. Presses Polytechniques et Universitaires Romandes, Lausanne, p 377
8. Kingery WD (1960) In: Introduction to ceramics. John Wiley and Sons, NewYork
9. Chartier T, Gervais T, Chermant L, Chermant JL, Coster M (1992) J Eur Ceram Soc 10:299
10. Mei S, Yang J, Ferreira JMF (2001) J Eur Ceram Soc 21:185
11. Evans AG (1982) J Am Ceram Soc 65:497
12. Scherer GW (1987) J Am Ceram Soc 70:719
13. Rahaman MN, Jonghe LC (1987) J Am Ceram Soc 70:C348
14. Hong W, Dharani LR (1995) J Am Ceram Soc 78:1593
15. Boccaccini AR, Olevsky EA (1999) J Mater Process Technol 96:92